CrossMark
click for updates

Drude and Kukharskii mobility of doped semiconductors extracted from Fourier-transform infrared ellipsometry spectra

Stefan Zollner,[a] Pablo P. Paradis, Farzin Abadizaman, and Nuwanjula S. Samarasingha
Department of Physics, New Mexico State University, P.O. Box 30001, Las Cruces, New Mexico 88003

(Received 13 November 2018; accepted 13 December 2018; published 8 January 2019)

The factorized plasmon-phonon polariton description of the infrared dielectric function is generalized to include an additional factor to account for the effects of interband electronic transitions. This new formalism is superior to the usual Drude–Lorentz summation of independent oscillators, especially in materials with large transverse-longitudinal optical phonon splittings, multiple infrared-active phonon modes, or high concentrations of free carriers, if a broadband description of the dielectric function from the far-infrared to the vacuum-ultraviolet spectral region is desired. After a careful comparison of both approaches, the factorized description is applied to the dielectric function of undoped and doped semiconductors (GaAs, GaSb, and InAs) and metal oxides from 0.03 to 9.0 eV. Specifically, the authors find that both descriptions of the far-infrared dielectric function yield the same carrier density and mobility, at least for a single species of carriers. To achieve valid results for moderately high doping concentrations, measurements to lower energies would be helpful. *Published by the AVS.*
https://doi.org/10.1116/1.5081055

I. INTRODUCTION

The infrared optical spectra of semiconductors obtained from Fourier-transform infrared (FTIR) ellipsometry measurements contain rich information about their free carrier and lattice vibrational properties, such as the plasma frequency, carrier density, mobility, and energies and broadenings of transverse and longitudinal optical (LO) phonons.[1] There have been many discussions in the literature whether the dielectric function $\epsilon(\omega)$ should be written as a Drude–Lorentz sum of the contributions of various elementary excitations (such as plasmons, phonons, polaritons, excitons, etc.) or as a Berreman–Unterwald product of these terms. In this paper, we introduce a broadband factorized description of the dielectric function, which can be used from the far-infrared to the vacuum-ultraviolet spectral region, and apply it to undoped bulk cubic GaAs, wurtzite ZnO, and other materials. We also show that the factorized (Kukharskii) description of the infrared dielectric function for doped GaAs yields a similar electron concentration and mobility as the more commonly applied Drude–Lorentz model, if experimental errors and our limited experimental range (0.031–6.5 eV) are properly taken into account.

II. MODEL DIELECTRIC FUNCTIONS

A. Drude–Lorentz model (sum)

Following Helmholtz,[2] Kettler,[3] and Drude,[4–6] one can write the dielectric function $\epsilon(\omega)$ versus angular frequency ω as a sum

$$\epsilon(\omega) = 1 + \chi_{\mathrm{Drude}}(\omega) + \chi_{\mathrm{TO}}(\omega) + \chi_{\mathrm{electronic}}(\omega), \tag{1}$$

where the constant 1 is the contribution of the vacuum, the first term is

$$\chi_{\mathrm{Drude}}(\omega) = -\sum_i \frac{\omega_{u,i}^2}{\omega^2 + i\gamma_{D,i}\omega}, \tag{2}$$

the susceptibility of free carriers, the second term is

$$\chi_{\mathrm{TO}}(\omega) = \sum_i \frac{A_i \omega_{\mathrm{TO},i}^2}{\omega_{\mathrm{TO},i}^2 - \omega^2 - i\gamma_{\mathrm{TO},i}\omega}, \tag{3}$$

the susceptibility of transverse optical (TO) phonons, and the last term is

$$\chi_{\mathrm{electronic}}(\omega) = \sum_i \frac{B_i \omega_{0,i}^2}{\omega_{0,i}^2 - \omega^2 - i\gamma_{0,i}\omega}, \tag{4}$$

the susceptibility of bound carriers due to interband optical transitions.

The justification for this summation (1) is the electromagnetic superposition principle: we assume that the polarization fields of various charges under the influence of the external electric field of the light source can be added, because they are independent of each other, ignoring interactions between charges.

As suggested by Drude,[4,6] we allow more than one species i of free carriers with an unscreened (angular) plasma frequency[7]

$$\omega_{u,i}^2 = \frac{n_i e^2}{\epsilon_0 m_i^* m_0}, \tag{5}$$

Drude scattering rate $\gamma_{D,i}$, carrier density n_i, and effective mass m_i^* to contribute to the dielectric function. e is the electronic charge, ϵ_0 is the vacuum permeability, and m_0 is the free electron mass. Usually, just a small number of free carrier species (often one or two) are sufficient to describe $\epsilon(\omega)$, such as electrons and holes, light and heavy holes, electrons in different conduction band valleys, s- and d-electrons, or

Note: This paper is part of the Conference Collection: 8th International Conference on Spectroscopic Ellipsometry 2019, ICSE.
[a]Electronic mail: zollner@nmsu.edu; URL: http://ellipsometry.nmsu.edu

bulk and surface electrons. For n-type semiconductors with a single occupied conduction band valley or for metals with a simple spherical Fermi surface, only one term should be sufficient, while more terms might be needed for more complex Fermi surfaces of metals.

In the lattice absorption term (3), $\omega_{\mathrm{TO},i}$ is the (angular) TO phonon frequency with scattering rate $\gamma_{\mathrm{TO},i}$ and dimensionless oscillator strength A_i. Since electromagnetic waves are transverse, only TO phonons (not LO phonons) lead to a pole in the lattice susceptibility (3).

Similarly, in the interband absorption term (4) due to bound carriers, $\omega_{0,i}$ is the (angular) frequency of the transition, $\gamma_{0,i}$ is its scattering rate,[8] and B_i is its dimensionless oscillator strength. The summation in Eq. (3) runs over all infrared-active phonon modes in the crystal (usually a small number, much less than three times the number of atoms in the primitive unit cell), but additional modes may be required due to higher-order phonon absorption or impurity-related vibrational modes.[1]

The summation in Eq. (4) in principle runs over all $\vec{k}$-vectors in the Brillouin zone and all possible combinations of interband transitions. Therefore, the interband contribution is usually replaced by a summation

$$\chi_{\mathrm{electronic}}(\omega) = \sum_i g_i(\omega) \tag{6}$$

over a much smaller number of Kramers–Kronig-consistent general oscillator functions $g_i(\omega)$, which might include Lorentzians with complex (or even negative) amplitudes, Gaussians, Tauc–Lorentz, or Cody–Lorentz lineshapes, or the Herzinger–Johs parametric oscillator model.[9]

Writing the dielectric function as a sum of Lorentzians or other lineshapes as in Eq. (1) implies that the various contributions are independent and that there is no cross-talk (interaction) between different transitions. Therefore, these models only use one broadening parameter for each term, in each denominator.

If we are only interested in the infrared portion of the dielectric function spectrum, we can define the high-frequency dielectric constant

$$\epsilon_\infty = 1 + \lim_{\omega\to 0} \sum_i g_i(\omega). \tag{7}$$

This quantity describes the contribution of the vacuum and the electronic interband transitions to the static dielectric constant $\epsilon_s = \epsilon(\omega = 0)$. Experimentally, one obtains ϵ_∞ for insulators by measurements at frequencies above the region of lattice absorption (thus the subscript ∞) but far below the band gap. The infrared dielectric function then becomes

$$\begin{aligned}\epsilon_{\mathrm{IR}}(\omega) &= \epsilon_\infty - \sum_i \frac{\omega_{u,i}^2}{\omega^2 + i\gamma_{D,i}\omega} + \sum_i \frac{A_i\omega_{\mathrm{TO},i}^2}{\omega_{\mathrm{TO},i}^2 - \omega^2 - i\gamma_{\mathrm{TO},i}\omega} \\ &= \epsilon_\infty\left(1 - \sum_i \frac{\omega_{P,i}^2}{\omega^2 + i\gamma_{D,i}\omega}\right) + \sum_i \frac{A_i\omega_{\mathrm{TO},i}^2}{\omega_{\mathrm{TO},i}^2 - \omega^2 - i\gamma_{\mathrm{TO},i}\omega},\end{aligned} \tag{8}$$

where we have introduced the screened (angular) plasma frequency

$$\omega_{P,i}^2 = \frac{n_i e^2}{\epsilon_0\epsilon_\infty m_i^* m_0} = \frac{\omega_{u,i}^2}{\epsilon_\infty}. \tag{9}$$

We will use Eq. (8) to fit the infrared dielectric function of undoped and doped GaAs.[10,11]

For $\omega = 0$, Eq. (8) shows that in the absence of free carriers, the amplitudes A_i describe the contribution of lattice absorption to the static dielectric constant since[12]

$$\epsilon_s = \epsilon_\infty + \sum_i A_i. \tag{10}$$

For a single phonon absorption band, we can use the Lyddane–Sachs–Teller (LST) relation[13]

$$\epsilon_s = \epsilon_\infty \frac{\omega_{\mathrm{LO}}^2}{\omega_{\mathrm{TO}}^2} \tag{11}$$

to calculate the LO phonon frequency

$$\omega_{\mathrm{LO}} = \omega_{\mathrm{TO}}\sqrt{1 + \frac{A}{\epsilon_\infty}}. \tag{12}$$

(Kurosawa[14] and Barker[12] generalized the LST relation for cubic materials with multiple phonons and Schubert[15] for anisotropic crystals.)

In the presence of free carriers, the dielectric function (1) diverges at low frequencies. It is convenient to introduce the complex optical conductivity

$$\sigma(\omega) = -i\epsilon_0\omega[\epsilon(\omega) - 1], \tag{13}$$

which cancels the divergence of the Drude term and therefore remains finite at low frequencies. We can then identify the quantity

$$\sigma_{\mathrm{DC}} = \lim_{\omega\to 0} \sigma(\omega) \tag{14}$$

with the electrical low-frequency conductivity. For the specific case of the Drude–Lorentz model (8), we find

$$\sigma_{\mathrm{DC}} = \epsilon_0\epsilon_\infty \sum_i \frac{\omega_{P,i}^2}{\gamma_{D,i}} = \frac{e^2}{m_0}\sum_i \frac{n_i}{m_i^*\gamma_{D,i}} = \sum_i n_i e\mu_i. \tag{15}$$

A similar expression was already given by Drude.[4] The mobility of the carrier species i is given by[7]

$$\mu_i = \frac{e}{m_i^* m_0 \gamma_{D,i}} = \frac{e\tau_{D,i}}{m_i^* m_0}, \tag{16}$$

where $\tau_{D,i} = \gamma_{D,i}^{-1}$ is the Drude collision time.

B. Kukharskii model (product)

Berreman and Unterwald[16] take a completely different approach in their description of the dielectric function. Without making physical assumptions about the line shape of oscillators, they start with the mathematical fact that the dielectric function, like any analytic function in the complex plane, is completely determined by its zeroes and poles and therefore can be written as a quotient of two polynomials. Since $\epsilon(\omega)$ approaches unity as the angular frequency goes to infinity, the

number of poles must be equal to the number of zeroes and the highest-order polynomial coefficients in the numerator and denominator must be equal. Considering also the symmetry $\epsilon(-\omega)=\epsilon^*(\omega)$ to ensure that the time-dependent dielectric displacement remains real, poles and zeroes come in pairs and those not located on the imaginary axis must be symmetric relative to the imaginary axis. This results in the functional form[17]

$$\epsilon(\omega)=\prod_i \frac{\omega_{\mathrm{L},i}^2-\omega^2-i\gamma_{\mathrm{L},i}\omega}{\omega_{\mathrm{T},i}^2-\omega^2-i\gamma_{\mathrm{T},i}\omega}, \tag{17}$$

which was frequently applied to model the infrared reflectance of insulators.[18] For insulators with many phonon modes or for large TO/LO splittings, it often gives a better description than the Drude–Lorentz model of independent oscillators.[19,20]

Since the dielectric function $\epsilon(\omega)$ and its inverse $\epsilon^{-1}(\omega)$ (called the loss function) obey causality (i.e., the polarization response follows the applied electric field), both zeroes and poles must be located below the real axis in the complex plane, which is equivalent to the condition that all scattering rates $\gamma_{T,i}$ and $\gamma_{L,i}$ must be positive. (We assume a time-dependence $\exp(-i\omega t)$ for the electromagnetic wave. The other choice for the time-dependence $\exp(i\omega t)$ leads to complex conjugate equations with poles and zeroes above the real axis, see Barker).[12]

To understand the physical significance of the zeroes and poles in Eq. (17), it is instructive to place the various factors into three groups

$$\epsilon(\omega)=\epsilon(\omega)_{\mathrm{Drude}}\epsilon(\omega)_{\mathrm{TO}}\epsilon(\omega)_{\mathrm{electronic}}. \tag{18}$$

Berreman and Unterwald[16] already recognized that the Drude response of free carriers can be described by

$$\epsilon(\omega)_{\mathrm{Drude}}=\prod_i \frac{\omega_{\mathrm{LP},i}^2-\omega^2-i\gamma_{\mathrm{LP},i}\omega}{-\omega^2-i\gamma_{K,i}\omega}, \tag{19}$$

which corresponds to one pole at the origin and another one at $-i\gamma_{K,i}$. We chose the subscript K after Kukharskii, who first applied Eq. (19) to describe the reflectance of doped GaAs.[21,22] The zeroes in Eq. (19) are related to the lower longitudinal plasmon-phonon polaritons (LP).[1,23,24] In the absence of free carriers, the LP angular frequency vanishes and the Drude factor (19) becomes unity.

The second factor

$$\epsilon(\omega)_{\mathrm{TO}}=\prod_i \frac{\omega_{\mathrm{UP},i}^2-\omega^2-i\gamma_{\mathrm{UP},i}\omega}{\omega_{\mathrm{TO},i}^2-\omega^2-i\gamma_{\mathrm{TO},i}\omega} \tag{20}$$

describes the dielectric response of infrared lattice absorption. The poles are related to TO phonons, while the zeroes are the upper longitudinal plasmon-phonon polaritons (UP). In the absence of free carriers, the UP modes are the LO phonons. They are pushed toward higher energy by the interaction with longitudinal plasmon oscillations of free carriers.[23,24] (Since the plasmon oscillations are longitudinal, they interact only with the LO, but not with the TO phonons.) Additional factors may be attached to describe higher-order phonon absorption or impurity-related absorption.

For a single plasmon-phonon polariton mode, the lower and upper polariton frequencies are related to the screened plasma frequency and the LO frequency by[22,23]

$$\omega_P=\frac{\omega_{\mathrm{LP}}\omega_{\mathrm{UP}}}{\omega_{\mathrm{TO}}}, \tag{21}$$

$$\omega_{\mathrm{LO}}^2=\omega_{\mathrm{LP}}^2+\omega_{\mathrm{UP}}^2-\omega_P^2. \tag{22}$$

The third factor

$$\epsilon(\omega)_{\mathrm{electronic}}=\prod_i \frac{\omega_{\mathrm{L},i}^2-\omega^2-i\gamma_{\mathrm{L},i}\omega}{\omega_{0,i}^2-\omega^2-i\gamma_{0,i}\omega} \tag{23}$$

can be expressed as a sum similar to Eq. (4)

$$\epsilon(\omega)_{\mathrm{electronic}}\approx 1+\sum_i \frac{B_i\omega_{0,i}^2+i\omega(\gamma_{0,i}-\gamma_{L,i})}{\omega_{0,i}^2-\omega^2-i\gamma_{0,i}\omega} \tag{24}$$

with the oscillator strength

$$B_i=\frac{\omega_{L,i}^2}{\omega_{0,i}^2}-1, \tag{25}$$

if we pretend that all broadenings are small and thus neglect the coupling between different interband transitions. (The presence of broadenings justifies complex Lorentzian amplitudes.) More conveniently, we write this factor (24) as a sum of general oscillators

$$\epsilon(\omega)_{\mathrm{electronic}}=1+\sum_i g_i(\omega), \tag{26}$$

just like in the Drude–Lorentz case (6). We use the same definition (7) for ϵ_∞. If we are only interested in the dielectric function of doped insulators well below the band gap, this allows us to write

$$\epsilon_{\mathrm{IR}}(\omega)=\epsilon_\infty\prod_i \frac{\omega_{\mathrm{LP},i}^2-\omega^2-i\gamma_{\mathrm{LP},i}\omega}{-\omega(\omega+i\gamma_{K,i})}\prod_j \frac{\omega_{\mathrm{UP},j}^2-\omega^2-i\gamma_{\mathrm{UP},j}\omega}{\omega_{\mathrm{TO},j}^2-\omega^2-i\gamma_{\mathrm{TO},j}\omega}, \tag{27}$$

which is known as Kukharskii's equation.[21,22]

From the Kukharskii model (27), we can calculate the DC conductivity defined by Eq. (14) as

$$\sigma_{\mathrm{DC}}=\epsilon_0\epsilon_\infty\prod_i \frac{\omega_{\mathrm{LP},i}^2}{\gamma_{K,i}}\prod_j \frac{\omega_{\mathrm{UP},j}^2}{\omega_{\mathrm{TO},j}^2}. \tag{28}$$

It is not straightforward to break up this product into a sum of contributions of different species of carriers to the DC conductivity, but for a single carrier species, we can write using Eq. (21)

$$\mu=\frac{\sigma_{\mathrm{DC}}}{ne}=\frac{\epsilon_0\epsilon_\infty}{ne}\frac{\omega_{\mathrm{LP}}^2\omega_{\mathrm{UP}}^2}{\gamma_K\omega_{\mathrm{TO}}^2}=\frac{e}{m_0m^*\gamma_K}, \tag{29}$$

which is exactly the same expression as in the Drude–Lorentz case (16). The Drude and Kukharskii scattering rates are therefore the same and we can omit this distinction.

III. EXPERIMENTAL PROCEDURE

In the infrared spectral region, we acquired the ellipsometric angles ψ and Δ as a function of angular frequency ω on a J. A. Woollam FTIR variable angle of incidence spectroscopic ellipsometer (FTIR-VASE) from 0.031 to 0.600 eV with a resolution of 4 cm^{-1}, usually at five equally spaced angles of incidence from 60° to 80°. We performed two-zone measurements with two polarizer angles ($\pm$45°), two analyzer angles (0° and 180°) and a rotating compensator (15 spectra per revolution, 20 FTIR scans per spectrum). We also acquired ψ and Δ from 0.50 to 6.60 eV with 0.01 eV steps at the same angles of incidence on a J.A. Woollam VASE ellipsometer equipped with a computer-controlled Berek wave plate compensator.

Since data from these two instruments were merged, small discrepancies can be noticed in the region of overlap, possibly due to slight misalignment. Most noticeably, the data taken with the FTIR ellipsometer are noisy above 0.5 eV.

IV. RESULTS AND DISCUSSION

A. Intrinsic and n-type GaAs, doped GaSb, and InAs

In Fig. 1, we show the pseudodielectric functions for a nominally undoped (intrinsic) and a Si-doped (n-type) GaAs substrate from 0.031 to 6.5 eV. Above 1 eV, we used tabulated optical constants for undoped and n-type GaAs and its native oxide taken from the literature.[25–27] This allowed us to determine the native oxide thickness (40 and 26 Å, respectively). This fit is generally quite good although some discrepancies were found, most likely due to polishing damage near the surface and uncertainties in the optical constants of the native oxide.[27]

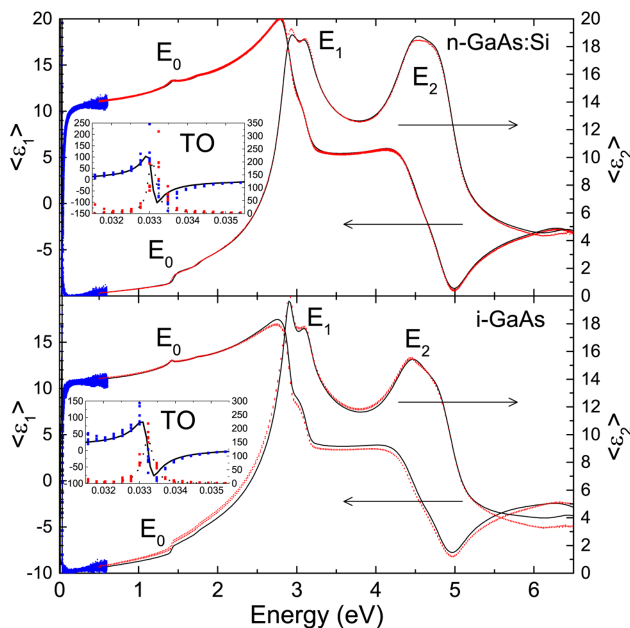

FIG. 1. Real and imaginary parts of the pseudodielectric function for silicon-doped (top) and undoped (bottom) GaAs covered with native oxide. Data from two different instruments were merged. The insets show expanded views of the regions of lattice absorption. Symbols show experimental data, lines the best fit to Eq. (18) with parameters given in Table I.

Using the tabulated optical constants for the electronic part of the dielectric function $\epsilon_{\text{electronic}}(\omega)$, we then fitted the remaining parameters (TO phonon and polariton energies and broadenings) in Eqs. (18) and (27), with results shown in Table I. ϵ_∞ was taken as the zero-energy limit of the tabulated dielectric functions.

Since the effects of plasmon-phonon polaritons on the optical constants can only be seen at the lowest photon energies, we also show the ellipsometric angle ψ below 0.09 eV for both substrates in Fig. 2. For each sample, there are two regions called *reststrahlen* bands (shown in gray), where ψ is close to 45° (and the normal-incidence reflectance is high). One of these bands extends from zero to E_{LP}, while the other one extends from E_{TO} to E_{UP}. Our FTIR ellipsometer has good sensitivity to E_{UP} (which appears as a strong peak in the loss function shown in Fig. S1) and its broadening. E_{TO} is right at the edge of our experimental range but clearly visible in ϵ, see the insets in Fig. 1. The energy range of the lower plasmon-phonon polariton band, on the other hand, is too low to be measurable using our instrument. Nevertheless, we obtain reasonable values for all relevant parameters, see Table I. The only exceptions are the Kukharskii and LP broadenings, which are strongly correlated.

Using Eqs. (21) and (22), we calculated the plasma and LO phonon frequencies. From $E_P = 13.0$ meV for undoped GaAs, we obtain a carrier density of 8.5×10^{16} cm^{-3}, which should be considered an upper limit. For n-type GaAs, $E_P = 36.7$ meV implies a carrier density of 6.8×10^{17} cm^{-3}, which is within the range of doping densities specified by the supplier (5.5–14×10^{17} cm^{-3}). An effective electron mass of $m_0 = 0.063$ was used.

For comparison, we also fitted the same data shown in Fig. 2 with the Drude–Lorentz model (8). The Drude and TO phonon energies and broadenings are also shown in Table I. The LO energy, carrier density, and mobility were calculated from Eqs. (12), (9), and (16), respectively. The carrier densities and LO frequencies agree quite well between both models. Also, the optical mobility for undoped and doped GaAs obtained from the Drude–Lorentz fit agrees with the electrical mobility expected for the given carrier concentration.[28]

Unfortunately, the Kukharskii scattering rate γ_K disagrees with the Drude scattering rate γ_D, comparing Eqs. (16) and (29), and therefore the Kukharskii mobilities are not reliable, see Table I. As mentioned earlier, this is due to our limited spectral range and the correlations in the fit between γ_K and γ_{LP} because of the larger number of broadening parameters in the Kukharskii model.

Results for *n*-type and *p*-type GaSb and for InAs are also listed in Table I and discussed in the supplementary material.[38]

B. Bulk undoped ZnO

According to Kukharskii,[22] the factorized dielectric function (18) can also be applied to each diagonal component of the dielectric tensor of anisotropic materials with at least orthorhombic symmetry, where the dielectric properties can be described by a diagonal tensor in a coordinate system that is invariant with photon energy.

TABLE I. Screened plasma frequency $E_P = \hbar\omega_P$, Drude broadening $\Gamma_D = \hbar\gamma_D$, high-frequency dielectric constant ϵ_∞, carrier density n, mobility μ, TO and LO phonon energies $E_{\rm TO} = \hbar\omega_{\rm TO}$ and $E_{\rm LO} = \hbar\omega_{\rm LO}$ and broadening $\Gamma_{\rm TO} = \hbar\gamma_{\rm TO}$, Kukharskii broadening $\Gamma_K = \hbar\gamma_K$, and lower and upper plasmon-polariton frequencies $E_{\rm LP} = \hbar\omega_{\rm LP}$ and $E_{\rm UP} = \hbar\omega_{\rm UP}$ and their broadenings $\Gamma_{\rm LP} = \hbar\gamma_{\rm LP}$ and $\Gamma_{\rm UP} = \hbar\gamma_{\rm UP}$ for undoped and n-type GaAs as well as n-type and p-type GaSb and InAs. For uniaxial undoped ZnO, values for the ordinary (o) and extraordinary (eo) parameters are listed separately. Quantities marked (f) were fixed during the fit, and those marked with an asterisk were taken from the literature. For each material, the top row (model DL) shows a fit with Eq. (8), where E_P, Γ_D, $E_{\rm TO}$, $\Gamma_{\rm TO}$, and ϵ_∞ are experimental values from ellipsometry data, whereas n, μ, and $E_{\rm LO}$ were calculated using Eqs. (9), (16), and (12); the bottom row (model KK) shows experimental values ϵ_∞, $E_{\rm TO}$, $\Gamma_{\rm TO}$, Γ_K, $E_{\rm LP}$, $E_{\rm UP}$, $\Gamma_{\rm LP}$, and $\Gamma_{\rm UP}$ determined from a fit to the ellipsometry data with Eq. (18), whereas E_P, $E_{\rm LO}$, n, and μ were calculated using Eqs. (21), (22), (9), and (29), respectively. Calculated quantities are shown in bold. The broadenings shown in italics show strong parameter correlations and therefore are not reliable.

Sample	Model	E_P (meV)	Γ_D (meV)	ϵ_∞ (1)	n (cm^{-3})	μ (cm/V s)	$E_{\rm TO}$ (meV)	$E_{\rm LO}$ (meV)	$\Gamma_{\rm TO}$ (meV)	Γ_K (meV)	$E_{\rm LP}$ (meV)	$E_{\rm UP}$ (meV)	$\Gamma_{\rm LP}$ (meV)	$\Gamma_{\rm UP}$ (meV)
u-GaAs	DL	12.4	4.2	10.8	**7.5 × 10^{16}**	**4400**	33.3	**35.9**	0.3					
u-GaAs	KK	**13.0**		10.8	**8.5 × 10^{16}**	**45 000**	33.2	**35.8**	0.3	*0.4*	11.9	36.2	*0.6*	0.3
n-GaAs	DL	35.6	5.4	11.0	**6.4 × 10^{17}**	**3400**	33.3	**35.6**	0.3					
n-GaAs	KK	**36.7**		11.0	**6.8 × 10^{17}**	**1600**	33.0	**35.0**	0.2	*11.3*	29.2	41.5	*4.9*	4.3
n-GaSb	DL	17	2 (f)	14.6	**1.8 × 10^{18}**	1000 (f)	27.78*	28.89*	0.3 (f)					
n-GaSb	KK	**10.9**		14.6	**7.2 × 10^{17}**	**1000**	27.78*	**28.3**	0.3 (f)	*2*	10.7	28.4	*1*	1 (f)
p-GaSb	DL	33.3	32.8	14.0	**3.4 × 10^{18}**	**120**	27.78*	28.89*	0.3 (f)					
p-GaSb	KK	**28.9**		14.0	**2.5 × 10^{18}**	**600**	27.78*	**28.6**	0.3 (f)	*6.4*	25.1	32.0	1 (f)	*11.7*
InAs	KK	**17**		12.2	**5.9 × 10^{16}**	**50 000**	27*	**30**	0.3 (f)	1 (f)	15	31	1 (f)	1 (f)
ZnO (o)	KK			3.73			50.7		1.2			73.2		1.1
ZnO (eo)	KK			3.81*			46.8		1 (f)			71.1		0.9

To illustrate this point, we analyze the ellipsometric angles and the pseudodielectric function of a bulk c-axis oriented ZnO substrate obtained commercially, see Fig. 3. To model these data, we use a uniaxial model for a bulk substrate with an ordinary and an extraordinary dielectric function, each described independently with the form given by Eq. (18). Since no free carrier effects are visible for this substrate, the Drude factor was set to unity. A surface roughness layer thickness (described with a 50/50 mixture of ZnO and voids using the Bruggeman effective medium approximation) of 21 Å was found from the magnitude of the pseudoabsorption below the band gap of about 3.1 eV. The electronic part of the ordinary dielectric function was described using two Tauc–Lorentz oscillators to account for the absorption of the main exciton triplet[29–31] (not resolved) and the exciton-phonon complexes.[29,32,33] At higher energies, we added two simplified Herzinger–Johs parametric oscillators and a pole at 11 eV. For our c-axis oriented ZnO substrate, the extraordinary dielectric function does not have a significant impact on the pseudodielectric function above the region of lattice absorption. We therefore assume that the electronic part of the extraordinary dielectric function is

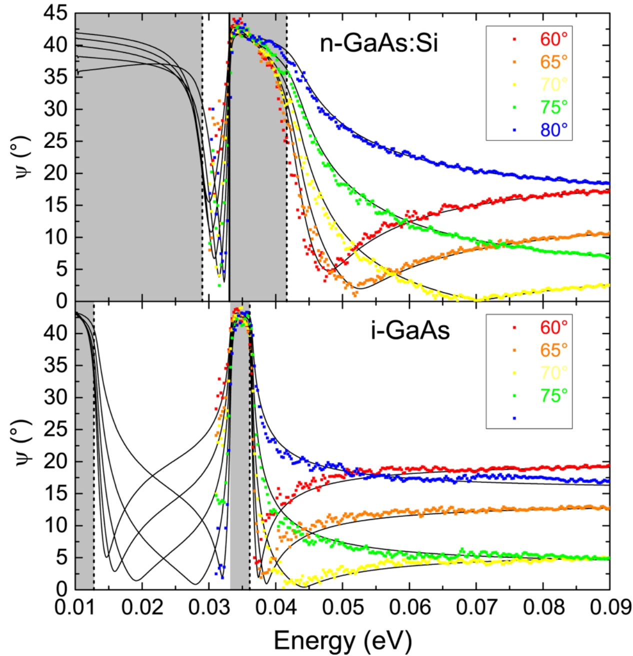

FIG. 2. Ellipsometric angle ψ at five angles of incidence for silicon-doped (top) and undoped (bottom) GaAs covered with native oxide in the region of plasmon-polariton absorption (gray). Symbols show experimental data, lines the best fit to Eq. (18) with parameters shown in Table I. The reststrahlen bands are shaded in gray.

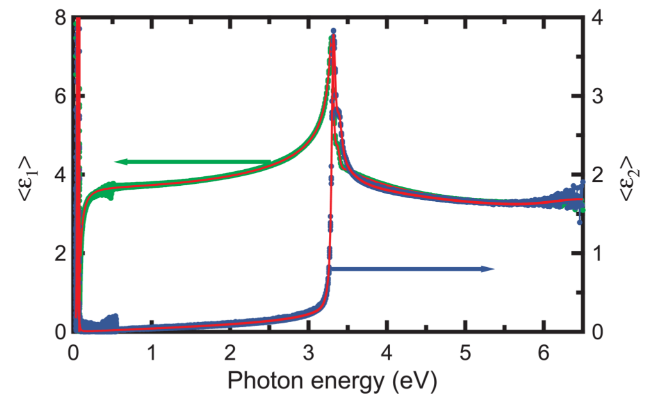

FIG. 3. Real and imaginary parts of the pseudodielectric function for undoped c-axis oriented bulk ZnO with 21 Å surface roughness. Data from two different instruments were merged. Points show experimental data, lines the best fit to Eq. (18) with parameters in Table I.

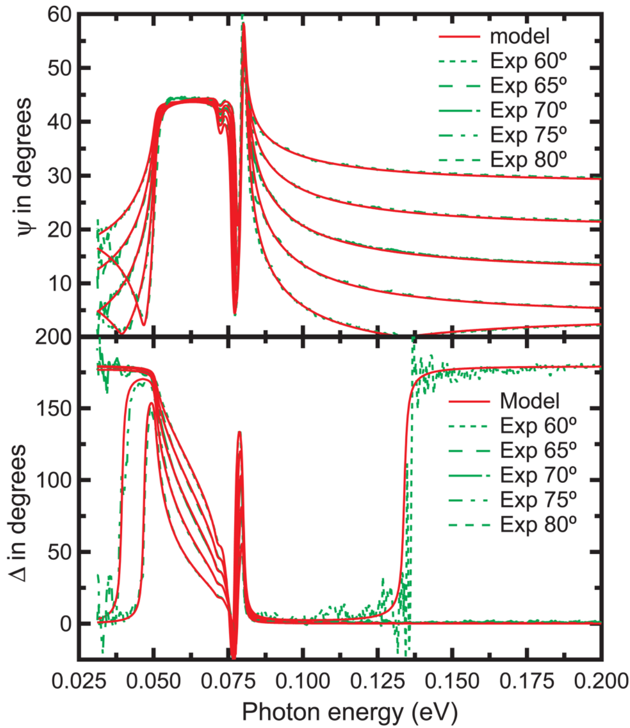

FIG. 4. Ellipsometric angles ψ and Δ for undoped c-axis oriented bulk ZnO with 21 Å surface roughness in the region of infrared lattice absorption. Points show experimental data, lines the best fit to Eq. (18) with parameters in Table I.

equal to that of the ordinary dielectric function, except for a rigid shift upward by 0.08, see Ref. 34. Our data are not sensitive to the complications described by Shokhovets *et al.*[35] The infrared lattice absorption of ZnO is dominated by the $E_1(A_1)$ phonons in the ordinary (extraordinary) dielectric function, each of which is split into a TO/LO pair by the Fröhlich interaction.[34]

Our experimental ellipsometry data for bulk ZnO along with the best fit using Eq. (18) in the low and high photon energy regions are shown in Figs. 3 and 4, respectively. The physical significance of various structures in the spectra has been explained elsewhere.[34] Our main point here is to show that Eq. (18) gives an excellent description over the complete spectral range from 0.03 to 6.5 eV. Our fit only has one problem: we are unable to describe the exact energy where the pseudo-Brewster angle of the sample changes from 0 to π. This energy depends on the precise value of the high-frequency dielectric constant ϵ_∞. In our approach, ϵ_∞ is not a free parameter, but determined by the electronic part of the spectrum shown in Fig. 3. A slight mismatch of the data from the two instruments causes a small error in ϵ_∞ (on the order of 0.05), which is responsible for the error seen near 0.14 eV in Fig. 4.

V. SUMMARY

Fifty years ago, modulation spectroscopy[36] (to study the electronic band structure of materials) and vibrational spectroscopy[1,37] (Raman and FTIR, especially) were distinctly different fields, with different approaches to describe experiments. The availability of modern commercial ellipsometry instruments covering the range from 0.03 to 9.0 eV requires a consistent broadband approach suitable for insulators, semiconductors, and metals. The Drude–Lorentz summation (1) meets the broadband requirement, but it is not suitable for interacting excitations, such as insulators with multiple phonons[19,20] or doped semiconductors with coupled longitudinal phonon-plasmon polaritons.[21,22] We therefore introduced a factorized formalism (17), a generalization of Kukharskii's equation (27), which is appropriate to describe insulators, semiconductors, and metals over the complete spectral range from the mid-IR to the vacuum-UV. This product (17) is easily implemented in commercial software. Several examples were given in the main text and in the supplementary material.[38]

Specifically, we also presented an approach to calculate the carrier mobility of doped semiconductors from Kukharskii's equation, if the effective mass of the carriers is known. We applied this approach to doped GaAs, InAs, and GaSb. Our results are reasonable, but the study of doped semiconductors could be more reliable if the lower spectral range of commercial FTIR ellipsometers could be extended to 0.01 eV.

ACKNOWLEDGMENTS

This paper is based, in part, on research sponsored by Air Force Research Laboratory (AFRL) (Agreement No. FA9453-18-2-0046). The work at NMSU was supported by the National Science Foundation (NSF) (No. DMR-1505172). The U.S. Government is authorized to reproduce and distribute reprints for governmental purposes notwithstanding any copyright notation thereon. The views and conclusions contained herein are those of the authors and should not be interpreted as necessarily representing the official policies or endorsements, either expressed or implied, of Air Force Research Laboratory (AFRL) and/or the US Government.

[1]M. Schubert, *Infrared Ellipsometry on Semiconductor Layer Structures: Phonons, Plasmons, and Polaritons* (Springer, Berlin, 2004).
[2]H. Helmholtz, Ann. Phys. **230**, 582 (1875).
[3]E. Kettler, Ann. Phys. **266**, 299 (1887).
[4]P. Drude, Physik. Z. **1**, 161 (1900), available at https://babel.hathitrust.org/cgi/pt?num=161&u=1&seq=6&view=image&size=100&id=mdp.39015068319667.
[5]P. Drude, *The Theory of Optics* (Longmans, Green, and Company, New York, 1902), p. 398.
[6]S. Roberts, Phys. Rev. **100**, 1667 (1955); **114**, 104 (1959).
[7]M. Schubert, T. Hofmann, and C. M. Herzinger, J. Opt. Soc. Am. A **20**, 347 (2003).
[8]S. Zollner, S. Gopalan, M. Garriga, J. Humlíček, L. Viña, and M. Cardona, Appl. Phys. Lett. **57**, 2838 (1990).
[9]T. N. Nunley, N. S. Fernando, N. Samarasingha, J. M. Moya, C. M. Nelson, A. A. Medina, and S. Zollner, J. Vac. Sci. Technol. B **34**, 061205 (2016).
[10]R. T. Holm, J. W. Gibson, and E. D. Palik, J. Appl. Phys. **48**, 212 (1977).
[11]J. Humlíček, R. Henn, and M. Cardona, Appl. Phys. Lett. **69**, 2581 (1996).
[12]A. S. Barker, Phys. Rev. **136**, A1290 (1964).
[13]R. H. Lyddane, R. G. Sachs, and E. Teller, Phys. Rev. **59**, 673 (1941).
[14]T. Kurosawa, J. Phys. Soc. Jpn. **16**, 1298 (1961).
[15]M. Schubert, Phys. Rev. Lett. **117**, 215502 (2015).
[16]D. W. Berreman and F. C. Unterwald, Phys. Rev. **174**, 791 (1968).

[17]R. P. Lowndes, Phys. Rev. B **1**, 2754 (1970).
[18]F. Gervais and B. Piriou, J. Phys. C Solid State Phys. **7**, 2374 (1974).
[19]T. Willett-Gies, E. DeLong, and S. Zollner, Thin Solid Films **571**, 620 (2014).
[20]C. J. Zollner, T. Willett-Gies, S. Zollner, and S. Choi, Thin Solid Films **571**, 689 (2014).
[21]A. A. Kukharskii, Fiz. Tverd. Tela **14**, 1744 (1972) [Sov. Phys. Solid State **14**, 1501 (1972).
[22]A. A. Kukharskii, Solid-State Commun. **13**, 1761 (1973).
[23]A. Mooradian and G. B. Wright, Phys. Rev. Lett. **16**, 999 (1966).
[24]A. Mooradian and A. L. McWhorter, Phys. Rev. Lett. **19**, 849 (1967).
[25]S. Zollner and D. Zarr, *2000 IEEE International Symposium on Compound Semiconductors*, edited by M. Melloch and M. A. Reed (IEEE, Piscataway, NJ, 2000), p. 251.
[26]S. Zollner, J. Appl. Phys. **90**, 515 (2001).
[27]S. Zollner, Appl. Phys. Lett. **63**, 2523 (1993).
[28]D. L. Rode and S. Knight, Phys. Rev. B **3**, 2534 (1971).
[29]S. Shokhovets, O. Ambacher, B. K. Meyer, and G. Gobsch, Phys. Rev. B **78**, 035207 (2008).
[30]H. Yoshikawa and S. Adachi, Jpn. J. Appl. Phys. **36**, 6237 (1997).
[31]M. D. Neumann, N. Esser, J.-M. Chauveau, R. Goldhahn, and M. Feneberg, Appl. Phys. Lett. **108**, 221105 (2016).
[32]S. Shokhovets, G. Gobsch, and O. Ambacher, Superlattices Microstruct. **39**, 299 (2006).
[33]M. D. Neumann, C. Cobet, N. Esser, B. Laumer, T. A. Wassner, M. Eickoff, M. Feneberg, and R. Goldhahn, J. Appl. Phys. **110**, 013520 (2011).
[34]N. Ashkenov *et al.*, J. Appl. Phys. **93**, 126 (2003).
[35]S. Shokhovets, L. Spieß, and G. Gobsch, J. Appl. Phys. **107**, 023509 (2010).
[36]M. Cardona, *Modulation Spectroscopy* (Academic, New York, 1969).
[37]M. Cardona, *Light Scattering in Solids I* (Springer, Berlin, 1983).
[38]See supplementary material at https://doi.org/10.1116/1.5081055 for additional experimental data and discussion of *n*- and *p*-type GaSb, InAs, and spinel ($MgAl_2O_4$).

Supplementary Materials: Drude and Kukharskii Mobility of Doped Semiconductors Extracted from Fourier-Transform Infrared Ellipsometry Spectra

(Dated: 3 December 2018)

Stefan Zollner,[1] Pablo P. Paradis,[1] Farzin Abadizaman,[1] and Nuwanjula S. Samarasingha[1] [1)] *Department of Physics, New Mexico State University, P.O. Box 30001, Las Cruces, NM 88003*

S1. DEFINITION OF THE PSEUDO-DIELECTRIC FUNCTION

As described in the main manuscript, each isotropic pure material is characterized by a frequency-dependent dielectric function $\epsilon(\omega)$. A sample in an ellipsometry experiment consists of more than one material (even a bulk material will have a surface region with optical constants different from the bulk) and therefore is described by ellipsometric angles ψ and Δ and a Fresnel reflectance ratio

$$\rho = \tan\psi \exp(i\Delta), \tag{S1}$$

which depend on the optical constants of all materials and the thicknesses of all layers (Fujiwara 2006).

The pseudo-dielectric function of a bulk material with a very thin surface overlayer defined by

$$\langle\epsilon(\omega)\rangle = \sin^2\phi\left[1+\tan^2\phi\left(\frac{1-\rho}{1+\rho}\right)^2\right], \tag{S2}$$

where ϕ is the angle of incidence, is a zero-order approximation of the dielectric function $\epsilon(\omega)$ of the bulk material where the effects of the surface overlayer are ignored (Fujiwara 2006, Yu and Cardona 2010). If overlayers are thin, the pseudo-dielectric function does not usually depend on the angle of incidence and therefore is a good representation of experimental data. For thick layers on a substrate, it is better to display ellipsometric angles, since there is little resemblance of the pseudo-dielectric function to the dielectric functions of the constituent materials. (Kormondy 2014). We also display the ellipsometric angles in the infrared spectral region, where the pseudo-dielectric function is dominated by a few sharp peaks that obliterate smaller features in the data.

S2. RESULTS FOR GASB

We measured the ellipsometric angles for two commercial GaSb substrates. The first one was Te doped, to compensate the p-type nature of nominally undoped GaSb, where Ga vacancies and Sb antisite defects result in a hole concentration of about 10^{17} cm^{-3} (Kulala 2014). This Te doping resulted in an electron concentration of 4$-$6$\times10^{16}$ cm^{-3}, as specified by the supplier. Since the L-valleys in the conduction band of GaSb are just 70 meV about the Γ conduction band minimum, most electrons are expected to be in the L-valley at room temperature (Rode 1975), which has a density of states effective mass of 0.57. The effective mass in the Γ-valley is much smaller, only 0.041.

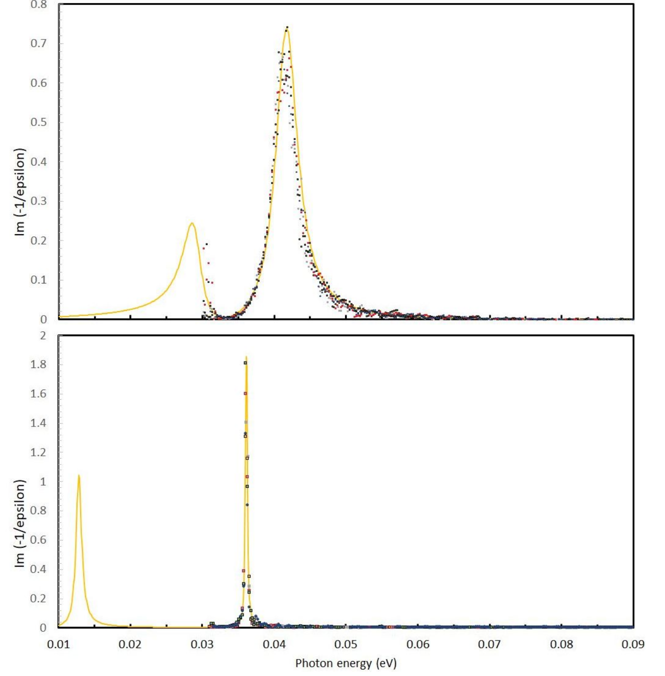

FIG. S1. Same data as in Fig. 2 for n-type GaAs (top) and undoped GaAs (bottom), but displayed as the loss function $-\mathrm{Im}(1/\epsilon)$. The line shows the model, the symbols the data. The LP and UP polariton modes are shown as peaks, shifting and broadening dependent on carrier concentration.

The other GaSb substrate was a zinc-doped p-type sample with a hole density greater than 10^{18} cm^{-3} specified by the supplier. Hole transport in GaSb is complicated because of k-linear terms due to the lack of inversion symmetry and the warped non-parabolic heavy and light hole bands (Heller 1985). To model this transport at room temperature with one band, an effective mass of 0.3 was chosen. The mobility expected for this sample is 200$-$450 cm^2/Vs.

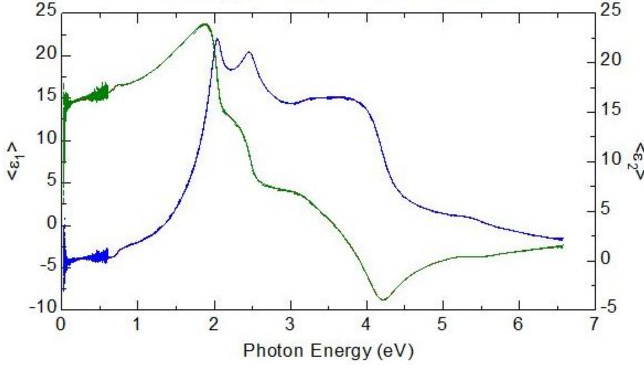

FIG. S2. As Fig. 1, but for n-type compensated bulk GaSb with an electron density of $4-6\times10^{16}$ cm^{-3}.

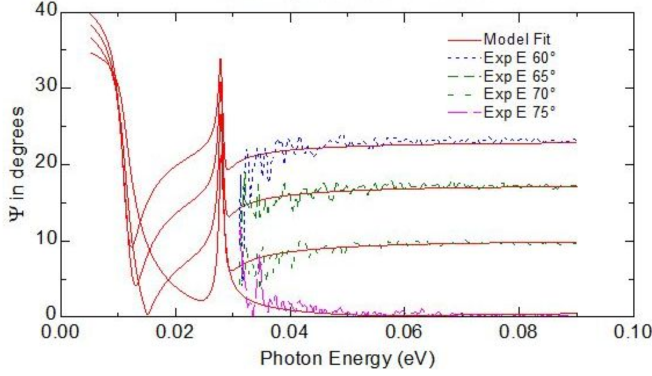

FIG. S3. As Fig. 2, but for n-type compensated bulk GaSb with an electron density of $4-6\times10^{16}$ cm^{-3}.

A. n-type GaSb with low doping

Studying GaSb was more challenging than GaAs, because no high-accuracy optical constants for bulk GaSb were available over the complete spectral range from 0.5 to 6.6 eV. We therefore acquired the pseudo-dielectric function, determined the oxide thickness (15 Å) from the pseudo-absorption below the band gap,[9] and then fitted GaSb optical constants using a parametric oscillator model. The results are shown in Fig. S2. Unfortunately, our results for ϵ of GaSb are quite different from the literature, presumably due to surface polishing damage of our commercial GaSb wafer. A high-frequency dielectric constant ϵ_∞=14.6 was found from these data, consistent with the literature.

The ellipsometric angle ψ in the mid-infrared is shown in Fig. S3. Despite the noise, it is clear that ψ is not flat, but shows some curvature. For angles of incidence ϕ between 60° and 70°, ψ bends down towards lower energies, while it bends up for ϕ=75°. For ϕ=75°, Δ also shows a phase change by π as the Brewster angle crosses the angle of incidence (not shown). To describe this curvature, we fix the TO phonon energy and its broadening as well as the UP broadening and fit the other parameters of the Kukharski model. The model fits the data well and the parameters are quite reasonable, see Table I. We find a plasma frequency of 10.9 meV from Eq. (21), which corresponds to a carrier density of 7.2×10^{17} cm^{-3} (an order of magnitude larger than the electron concentration specified by the supplier) for the L-valley effective mass of 0.57. This should be considered an upper limit. The upper limit of the electron concentration measurable with our FTIR-VASE instrument is an order of magnitude larger for n-type GaSb than for n-type GaAs, because the effective (L-valley) electron mass in GaSb is an order of magnitude larger than the effective (Γ-valley) mass in GaAs. The Kukharski broadening of Γ_K=2 meV has a large error bar, but it corresponds to a mobility of 1000 cm^2/Vs, which is quite reasonable for n-type GaSb at room temperature. (The manufacturer specifies mobilities in the range of 2000−3500 cm^2/Vs.) We also calculate an LO phonon energy of 28.3 meV from Eq. (22), which is just slightly lower than the accepted value of 28.9 meV.

We stress that the carrier density and mobility listed above used the L-valley effective mass of 0.57. If we instead used the Γ-valley effective mass of 0.041, this would result in a carrier concentration n=5.1×10^{16} cm^{-3} (within specifications) and a mobility of 14,000 cm^2/Vs (which is much too high).

To fit the data for n-type GaSb with the Drude-Lorentz model, we fix the TO energy at 27.78 meV and its broadening at 0.3 meV (instrumental resolution). We also calculate the amplitude A=1.19 from Eq. (12) using the value of 28.89 meV for the LO phonon energy. This leaves the plasma frequency and Drude broadenings as the only parameters, assuming an L-valley electron mass of 0.57. Since the Drude broadening trends to very small values in the fit (leading to unphysically high mobilities), we fix γ_D at 2 meV, which corresponds to a mobility of 1000 cm^2/Vs, just like for the Kukharskii model. The screened plasma frequency is the only remaining parameter. We find E_P=17 meV (independent of our choice of γ_D), which corresponds to an electron concentration of 1.8×10^{18} cm^{-3}, clearly much higher than expected.

We note that the curvature of ψ at the lowest photon energies has two contribution, due to TO phonon absorption and due to free carriers. The TO phonon contribution to ψ is known (since the TO and LO phonon energies are known and the broadening can be set to the instrumental resolution) and therefore the Drude contribution can be fitted with a single parameter (the electron contribution). Nevertheless, the sensitivity to the Drude contribution is small and therefore an actual determination of the carrier contribution would require measurements at longer wavelengths, beyond the TO energy of 27.78 meV. Perhaps the extrapolation of our data to longer wavelengths and the subtraction of the lattice absorption effect is the reason for our poor values for carrier concentration and mobility of n-type GaSb.

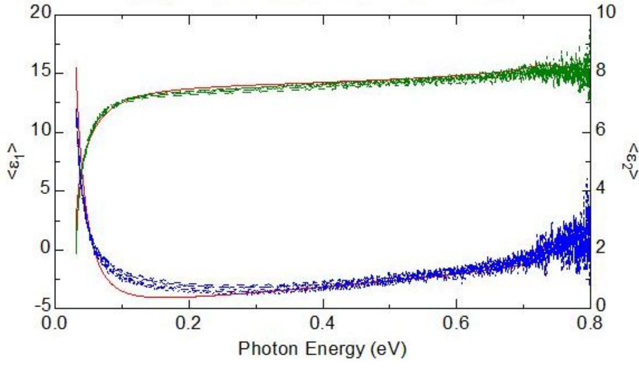

FIG. S4. As Fig. 1, but for p-type bulk GaSb with 6 nm native oxide and a hole density greater than 10^{18} cm^{-3}. The lines show the best fit with a single Drude term and fixed TO lattice absorption.

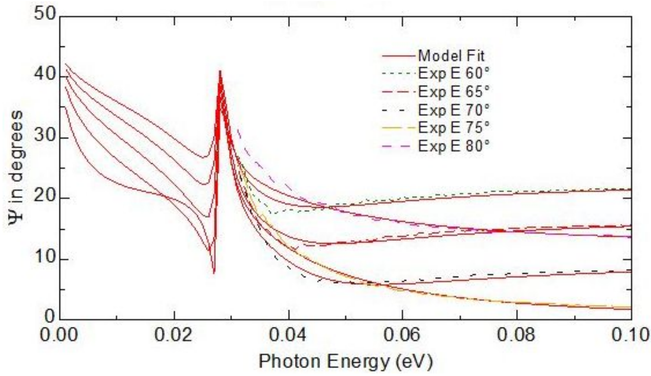

FIG. S5. As Fig. 2, but for p-type bulk GaSb with a hole density greater than 10^{18} cm^{-3}. The lines show the best fit with a single Drude term and fixed TO lattice absorption.

B. p-type GaSb with high doping

The effects of free carrier absorption are much more pronounced for the p-type sample with very high doping, see Fig. S4 (data above 0.8 eV are not available for this sample). We clearly see an increase of $\langle\epsilon_2\rangle$ and a decrease of $\langle\epsilon_1\rangle$ at the lowest energies, which is much larger than the expected phonon response. To fit these data with the Drude-Lorentz model, we fix the phonon parameters as stated above for the n-type sample. Figures S4 and S5 show the best fit with a single Drude term, leading to a hole concentration of 3.4×10^{18} cm^{-3} (with an effective hole mass of 0.3) and a mobility of 117 cm^2/Vs, which is quite reasonable. However, this fit is not very good. A much better fit can be obtained with two carrier species, a large term with a (screened) plasma frequency of 49.3 meV and Γ_D=318 meV (unreasonably large), and a smaller term with ω_P=26.5 meV and Γ_D=9.2 meV.

A Kukharskii fit using Eq. (27) with a single plasmon-phonon polariton (single hole species plus TO/LO phonon) yields a better fit than the Drude-Lorentz fit with a single type of holes. The parameters are shown

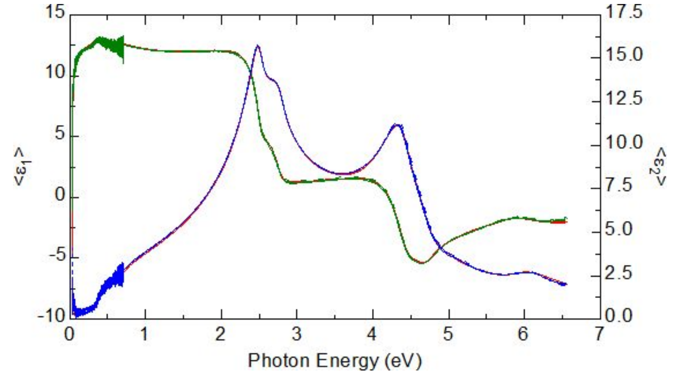

FIG. S6. As Fig. 1, but for nominally undoped InAs. Experimental data are shown by symbols (green-$\langle\epsilon_1\rangle$, blue-$\langle\epsilon_2\rangle$). Data from two instruments were merged. The lines show the best fit with Eq. (18), including one plasmon-phonon polariton and a parametric oscillator model to account for interband electronic transitions. The native oxide thickness is 6 nm.

in Table I. We find E_{LP}=25.1 meV and E_{UP}=32.0 meV, which yields a plasma frequency of E_P=28.9 meV and a carrier density of 2.5×10^{18} cm^{-3}, which is reasonable. The Kukharskii broadening is Γ_K=6.4 meV, which seems a bit small, yielding a high mobility of 600 cm^2/Vs. We were unable to find a better fit by adding a second plasmon to Eq. (27).

S3. RESULTS FOR INAS

Figure S6 shows the pseudo-dielectric function of nominally undoped InAs from 0.03 to 6.5 eV. The model for this wafer consists of a bulk InAs substrate and a 6 nm thick native oxide[27] (quite thick, no surface cleaning was attempted). The interband electronic transitions in the substrate are described using a semiconductor parametric oscillator model. Since prior experimental data for InAs are sparse below 1.5 and above 6 eV, we made small adjustments to the published model parameters, especially in the region near the direct band gap E_0, which can be seen clearly as an absorption threshold and a peak in $\langle\epsilon_1\rangle$ near 0.37 eV. Below E_0, $\langle\epsilon_2\rangle$ is about zero (except for the native oxide contribution to the pseudo-absorption), but $\langle\epsilon_1\rangle$ shows a clear drop below E_0. The high-frequency dielectric constant from our parametric model is ϵ_∞=12.2, close to its accepted value.

The FTIR-VASE data (below 0.7 eV) are noisier than in the near-IR, visible, and UV. Despite these noise issues, it is clear that there is a slow drop below 0.35 eV (due to the contribution of E_0 to the dielectric function) and then a sharp drop below 0.08 eV (due to plasmon-phonon polaritons).

We show a magnified graph of the far-IR data in Fig. S7. ψ is rather flat near 0.1 eV and drops slowly towards smaller energies, until reaching a minimum between 0.33 and 0.38 eV (depending on the angle of incidence). There is a very steep egde near 0.03 eV, where ψ reaches almost

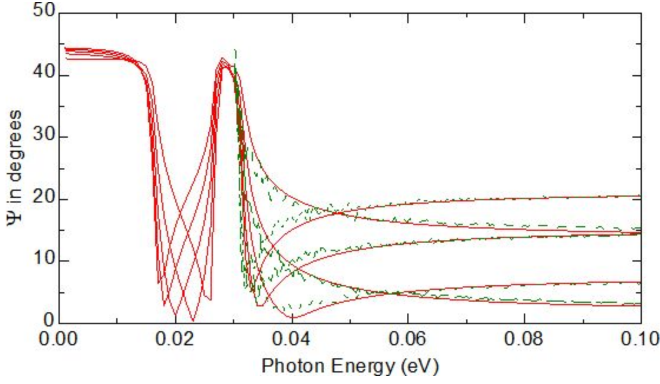

FIG. S7. As Fig. 2, but for nominally undoped InAs. The lines show the best fit with a single plasmon-phonon polariton to account for free carrier and lattice absorption.

45°. This is the upper edge of the second restrahlen band and indicates the upper phonon-plasmon polariton energy. Our model places the TO phonon of bulk InAs at 27 meV, since it is not affected by free carrier effects. We also fix its broadening at 0.3 meV (the instrumental resolution). The UP polariton is at 31 meV, significantly higher than the LO phonon energy of 29 meV. This is due to the polariton effects pushing the UP energy above the LO phonon energy because of free carrier effects (doping). We fix its broadening at 1 meV to get good agreement with the data. Finally, the LP polariton energy is 15 meV, well below our experimental range, also with a fixed broadening of 1 meV. We also fix the Kukharskii (mobility) broadening at 1 meV, since our data are not sensitive to this parameter.

The plasma frequency calculated from Eq. (21) is 17 meV, and the LO frequency calculated from Eq. (22) is 30 meV, only slightly higher than the accepted value of 29 meV. From the plasma frequency, we calculate an electron density of 5.9×10^{16} cm^{-3} for this nominally undoped sample, assuming an effective electron mass of 0.023 for InAs. Our Kukharskii broadening of 1 meV results in a mobility of 50000 cm^2/Vs, which is a little (but not much) too high (Karataev 1977), since we are not sensitive to the broadenings parameters in our InAs data. (Basic parameters for bulk InAs were taken from the Ioffe Institute web site.)

S4. RESULTS FOR SPINEL

To demonstrate that Eq. (18) can be applied over the complete spectral range from 0.03 to 9.0 eV, we present a new fit to data previously[20] published for spinel ($MgAl_2O_4$). In our previous work,[20] we used five TO/LO oscillators as in Eq. (20) to describe the infrared spectral region and two Tauc-Lorentz oscillators and a pole for the near-IR to vacuum-UV region. Both regions were fitted separately. The problem with this approach was that ϵ_∞ entered as a separate parameter in both fits and we

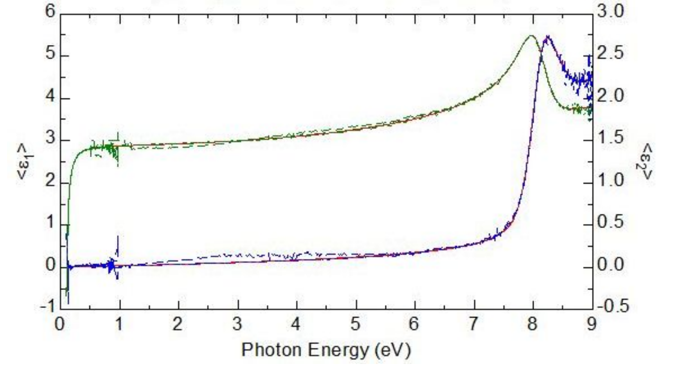

FIG. S8. Pseudodielectric function for spinel ($MgAl_2O_4$) with 16.4 Å surface roughness from the mid-IR to the vacuum-UV. Data are shown in green ($\langle\epsilon_1\rangle$) and blue ($\langle\epsilon_2\rangle$), the model fit using Eq. (18) in red. Two Tauc-Lorentz oscillators and a pole define the dispersion in this energy range.

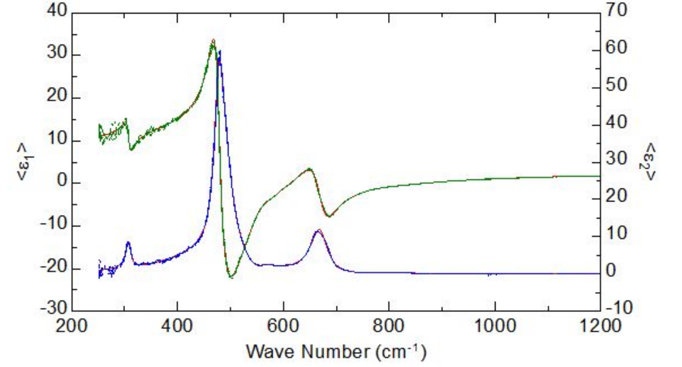

FIG. S9. As Fig. S8, but for the mid-infrared spectral range of spinel ($MgAl_2O_4$). Seven TO/LO phonon pairs as in Eq. (20) define the dispersion in this energy range.

had to make sure that it was consistent in both parts.

Our new Eq. (18) allows us to fit the entire dataset from 0.03 to 9.0 eV in one step. All parameters were adjusted simultaneously, including the surface roughness. To reduce the differences between data and fit, we increased the number of TO/LO phonon pairs from five to seven, but it is not clear if the two additional phonon modes are uniquely defined by the data. Results are shown in Figs. S8, S9, and S10. The Drude factor was set to unity for this insulator. Our revised parameters are very similar to those published previously[20] and therefore not listed again.

ADDITIONAL REFERENCES

- D. L. Rode, *Low-field electron transport* in *Semiconductors and Semimetals*, edited by R. K. Willardson and A. C. Beer (Academic Press, New York, 1975), Vol. 10, p. 1.
- V. V. Karataev, M. G. Milvidsky, N. S. Rytova, and V.

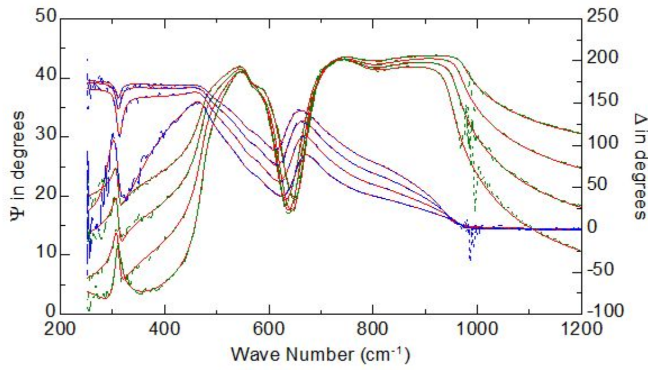

FIG. S10. As Fig. S9, but data are displayed as ellipsometric angles ψ (green) and Δ (blue) for four angles of incidence from 60° to 75°.

I. Fistui, Sov. Phys. Semicond. **11**, 1009 (1977).

- M. W. Heller and R. G. Hamerly, *Hole transport in gallium antimonide*, J. Appl. Phys. **57**, 4626 (1985).
- H. Fujiwara, *Spectroscopic Ellipsometry* (Wiley, Chichester, 2007).
- P. Y. Yu and M. Cardona, *Fundamentals of Semiconductors* (Springer, Berlin 2010).
- K. J. Kormondy, A. B. Posadas, A. Slepko, A. Dhamdere, D. J. Smith, K. N. Mitchell, T. I. Willet-Gies, S. Zollner, L. G. Marshall, J. Zhou, and A. A. Demkov, *Epitaxy of polar semiconductor Co_3O_4 (110): Growth, structure, and characterization*, J. Appl. Phys. **115**, 243708 (2014).
- J. Kujala, N. Segercrantz, F. Tuomisto, and J. Slotte, *Native point defects in GaSb*, J. Appl. Phys. **116**, 143508 (2014).